AD-A098 750 TEXAS UNIV AT AUSTIN F/G 20/10
THEORETICAL LOW ENERGY INELASTIC SCATTERING CROSS-SECTIONS FOR --ETC(U)
OCT 73 L LENAMON, J C BROWNE, R E OLSON N00014-75-C-0498
UNCLASSIFIED NL

END
DATE FILMED
8-81
DTIC

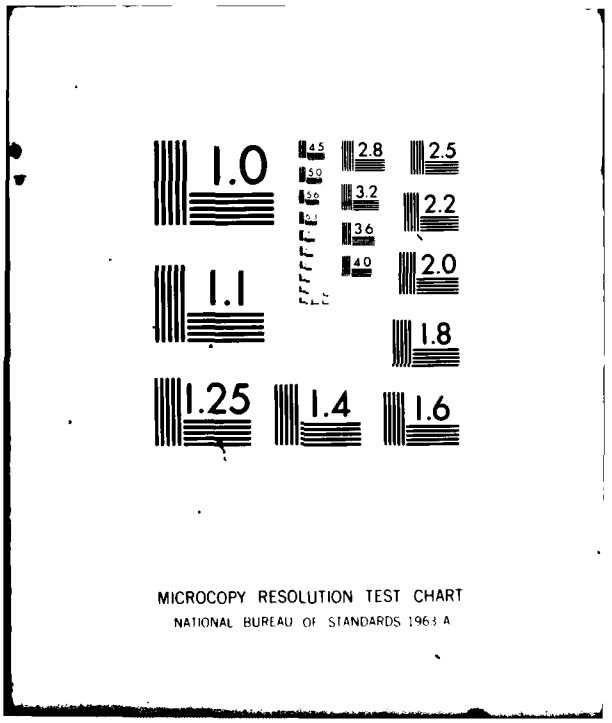
1.0
1.1
1.25
1.4
1.6
1.8
2.0
2.2
2.5
2.8
3.2
3.6
4.0
4.5
5.0
5.6
6.3
7.1
MICROCOPY RESOLUTION TEST CHART
NATIONAL BUREAU OF STANDARDS 1963 A

PHOTOGRAPH THIS SHEET

AD A098750

DTIC ACCESSION NUMBER

II

LEVEL

1

INVENTORY

THEORETICAL LOW ENERGY INELASTIC SCATTERING CROSS-SECTIONS FOR $He(2^3S) + He(1^1S) \rightarrow He(2^3P) + He(1^1S)$: CURVE-CROSSING BETWEEN THE $c^3\Sigma_g^+$ AND $b^3\Pi_g$ STATES OF He_2^*

DISTRIBUTION STATEMENT A
Approved for public release;
Distribution Unlimited

DISTRIBUTION STATEMENT

ACCESSION FOR
NTIS GRA&I ☑
DTIC TAB ☐
UNANNOUNCED ☐
JUSTIFICATION

PER LETTER

BY
DISTRIBUTION /
AVAILABILITY CODES

DIST	AVAIL AND/OR SPECIAL	
A		

DISTRIBUTION STAMP

DTIC
ELECTE
S MAY 7 1981 D
B

DATE ACCESSIONED

81 4 27 177

DATE RECEIVED IN DTIC

PHOTOGRAPH THIS SHEET AND RETURN TO DTIC-DDA-2

DTIC FORM OCT 79 70A

DOCUMENT PROCESSING SHEET

Submitted to Physical Review A

THEORETICAL LOW ENERGY INELASTIC SCATTERING CROSS-SECTIONS FOR $He(2^3S)$ + $He(1^1S) \rightarrow He(2^3P)$ + $He(1^1S)$: CURVE-CROSSING BETWEEN THE $c^3\Sigma_g^+$ AND $b^3\Pi_g$ STATES OF He_2‡

L. Lenamon and J. C. Browne
Departments of Computer Sciences and Physics
University of Texas at Austin, Austin, Texas

R. E. Olson
Molecular Physics Department
Stanford Research Institute, Menlo Park, California 94025

Low energy (5 -100 eV) cross sections have been computed for the inelastic scattering of $He(2^3S) + He(1^1S) \rightarrow He(2^3P) + He(1^1S)$. Two-state quantum-mechanical close-coupling calculations have been performed between the $c^3\Sigma_g^+$ and $b^3\Pi_g$ states of the He_2 molecule. The necessary molecular wavefunctions, potential curves, and rotational coupling matrix elements were obtained by ab initio computation. The inelastic transition probabilities are found to be quite large, $|S_{12}|^2 \approx 0.8 - 1.0$ for impact parameters close to the curve-crossing of the $c^3\Sigma_g^+$ and $b^3\Pi_g$ potential curves at $R_x \approx 3.3\ a_o$. The inelastic total cross-sections range from $1.0 \times 10^{-16} cm^2$ at 5 eV to $4.0 \times 10^{-16} cm^2$ at 100 eV. Reduced plots of the inelastic differential cross-sections show a sharp maximum at a $\tau = E\theta$ value of approximately 100 eV-deg. The strong inelastic process is also found to significantly alter the elastic differential cross-sections in the $\tau \approx 25$ -125 eV-deg region. The rotational coupling between the $c^3\Sigma_g^+$ and $b^3\pi_g$ states is found to be the dominant inelastic process at energies up to 500 eV.

---

‡ This research was supported by the Office of Naval Research under Contract No. N00014-67-0126-0017 and the National Science Foundation under Contract GA-33418. N00014-75-C-0498

Introduction

Low energy (E≈5-10 eV) differential scattering cross sections of $He(2^3S)$ on $He(1^1S)$ have been measured experimentally at Stanford Research Institute.[1] These cross sections show that there exists an inelastic loss process to the $He(2^3P) + He(1^1S)$ channel.[2]

Analysis of the He_2 potentials shown in Fig. 1 indicates that there are two possible inelastic channels for loss of the elastic flux at low collision energies. One possible channel is to a potential curve of the $^3\Sigma_g^+$ state that originates in $He(1s2p\ ^3P)$. This potential lies close to the $c^3\Sigma_g^+$ potential curve over a considerable range of internuclear separations. These two states are thus connected by radial $(\partial/\partial R)$ coupling matrix elements. This possible inelastic loss process has been studied previously by Evans, Cohen and Lane.[3] They find that the inelastic total cross-sections into the $^3\Sigma_g^+$ $He(1s2p\ ^3P) + He(1^1S)$ channel are very small at low energies ($Q = 5.0 \times 10^{-20} cm^2$ at 5 eV rising to only $7.7 \times 10^{-17}\ cm^2$ at 100 eV).

Another possible inelastic channel is the $b^3\Pi_g$ potential curve which also dissociates to $He(1s2p\ ^3P) + He(1s^2\ ^1S)$ and crosses the $c^3\Sigma_g^+$ potential curve at approximately $R_x = 3.3\ a_o$. These two curves lie within 0.5 eV for internuclear separations of $2.5\ a_o < R < 4.0\ a_o$. The coupling matrix element between these states is the rotational coupling operator, L_y. There is a reasonable intuitive basis for expecting this coupling to be substantial since both molecular states have 3p molecular orbital configurations. Thus this channel suggests itself as a source for substantial loss of flux from the $He(2^3S) + He(1^1S)$ elastic channel at low energies.

This paper presents close coupling computations on the molecular channels $c^3\Sigma_g^+$ and $b^3\Pi_g$ based on *ab initio* computed potential curves and coupling matrix elements. The computed inelastic total cross sections

are found to be very large ($Q > 10^{-16}$ cm^2 for $E \geq 5$ eV) and thus we strongly suggest that this inelastic channel represents the major loss process needed to explain the experimental observations.[2]

Wavefunctions, Potential Curves and Coupling Matrix Elements

The wavefunctions and potential cruves used to define the molecular channels for the cross-section computations were obtained by standard configuration interaction methods. The function used for the $c^3\Sigma_g^+$ state was a five configuration function Slater-type orbital basis set adapted from the work of Greenawalt.[4] The wavefunction is written as

$$\Psi_5(^3\Sigma_g^+) = c_1[1s^2;\ 1s'2s] + c_2[1s^2;\ 1s'2p_o] + c_3[1s^2;\ 1s'3s]$$

$$+ c_4[1s^2;\ 1s'3p_o] + c_5[1s^2;\ 1s'3d_o],$$

where, in this notation the orbitals to the left of the semicolon are on the ground state atom and those to the right the excited atom. The brackets denote the formation of an eigenfunction of L_z, S_z and S^2. The orbital exponents were optimized at each internuclear separation. The potential curve obtained by these computations was adjusted by the procedure of Klein, Greenawalt and Matsen.[5] The adjusted potential points are given in Table I along with the potential points available from the more elaborate computations of Kolker and Michels.[6]

The $b^3\pi_g$ potential curve was computed with a five configuration wavefunction

$$\Psi_5(b^3\pi_g) = c_1[1s^2;\ 1s2p_+] + c_2[1s^2;\ 1s3p_+]$$

$$+ c_3[1s^2;\ 1s''3d_+] + c_4[1s^2\ 1s';\ 3d_+] + c_5[\phi_1\phi_1;\ \phi_2\phi_3].$$

Here, ϕ_1 are elliptic orbitals; ϕ_1 passes to 1s in the united atom limit, while ϕ_2 and ϕ_3 pass to 2s and $3p_o$. The orbital exponents were optimized at each internuclear separation. The potential curve obtained by these computations was adjusted by the procedure of Klein, Greenawalt and Matsen.[4] The adjusted potential curve is given in Table I. The adjusted curves compare well with the RKR curves of Ginter and Battino.[7] A crossing point of $R_x = 3.29a_o$ is computed while Ginter and Battino show a crossing point of approximately $R_x = 3.2\ a_o$. The minima of both potential curves if somewhat larger than the experimental values.[7] The relative spacing seems to be in rather good agreement. The experimental value for the energy difference between the minima is 0.283315 a.u. while the computed value is 0.253315 a.u.

The coupling matrix elements $< {}^3\Sigma_g^+ \mid L_y \mid {}^3\Pi_g^- >$ were computed with the standard package of the Molecular Physics Group at the University of Texas at Austin. The coupling matrix elements were also computed with other rather different wavefunctions for several internuclear separations. The values (listed in Table I) are not sensitive to changes in the wavefunctions.

Scattering Cross Sections

In order to calculate the cross-sections, the potential points given in Table I were fit with a cubic spline function. The L_y coupling matrix elements were represented by the exponential form $L_y = 1.67 \times \exp(-0.231R)$ for internuclear separations $R \geq 2.77\ a_o$; within $2.77\ a_o$, L_y was set equal to 0.88. The transition probabilities and the real and imaginary parts of the S-matrix were then calculated at even ℓ (orbital angular momentum quantum number) values using the "amplitude-density" method of Secrest and Johnson.[8]

The calculated transition probabilities between the $c^3\Sigma_g^+$ and $b^3\Pi_g$ states are shown in Fig. 2. For convenience in comparing between energies, the transition probabilities are plotted versus impact parameter, b, where we have used the semiclassical relationship $b = (\ell + 1/2)/k$, in which the wavenumber $k = \sqrt{2\mu E/\hbar^2}$. At 5, 8.65, 10, and 25 eV, the coupled equations were solved for the transition probabilities at all even ℓ values so that the real and imaginary parts of the S-matrix could also be used for calculating the inelastic differential cross sections. However, at 100 eV the cost becomes prohibitive so we only solved the coupled equations at $\Delta\ell = 50$ intervals from $\ell = 100$ to $\ell = 700$. These are the points shown in Fig. 2.

Even at the lowest collision energy, 5 eV, the transition probabilities out of the $c^3\Sigma_g^+$ channel rise almost to unity. Furthermore, as the collision energy is increased, the inelastic process becomes quite appreciable at impact parameters larger than the crossing point at $R_x = 3.29a_o$. The reason can be seen by examining the dynamical nature of the rotational coupling matrix element that is given in an impact parameter formalism by

$$H_{12}(R) = vb\ L_y(R)/R^2$$

where v is the incident collision velocity. From Eq. (1) we can see that as the energy increases the coupling will become stronger and it will be possible to induce inelastic transitions at larger and larger impact parameters.

The transition probabilities display an unexpected oscillatory dependence around b = 1.5 a_0. There exists a region of stationary phase that causes a decrease in transition probability at b $\approx$ 1.5 a_0 at 5 eV and 25 eV and added "shoulders" at 8.65 and 10 eV. This effect is due to the difference potential between the $c^3\Sigma_g^+$ and $b^3\Pi_g$ states processing a maximum in the region about R = 1.5 a_0 (see Table I). We would therefore expect to see oscillations on the inelastic total cross sections due to this region of stationary phase in the phase differences.[9] However, for this case the oscillations will be very weak because of the dominance of the large impact parameter transition probabilities in the total cross section.

At both 25 and 100 eV there is a large increase in the transition probabilities at small impact parameters, b $\lesssim$ 1.0 a_0. This increase is due to a second crossing of the $c^3\Sigma_g^+$ and $b^3\Pi_g$ states at around 1.0 a_0 (Table I). The energy required to reach this region is approximately 18 eV so the effect is only observed at 25 and 100 eV. Since the wavefunctions used for constructing the potential curves were not set up to be extremely accurate at small internuclear separations, there may be some slight changes in the determination of the inner crossing. However, we may say with certainty that there is an inner crossing which will become important at high collision energies, E $\gtrsim$ 100 eV.

The inelastic total cross sections (the sum of both direct excitation and exchange excitation) were calculated by the summation

$$Q = \frac{\pi}{k^2} \sum_{\ell \text{ even}} (2\ell + 1)|S_{12}|^2 \qquad (2)$$

In Eq. (2) we have included a statistical weight factor of one half since one half of the incident flux is going into the nonreactive ungerade channel. At 100 eV the inelastic total cross-sections were evaluated by interpolating between the calculated transition probabilities. The calculated total cross sections are given in Table II and are displayed in Fig. 3. Also shown in Fig. 3 are the inelastic total cross sections calculated by Evans, Cohen, and Lane[3] for radial coupling to the $He(2^3P) + He(1^1S)$ state.

Our calculations can be extended to higher energies by using the method of Russek.[10] Inserting our potential parameters for the outer crossing at $R_x = 3.29a_o$, we obtain the cross sections shown by the dashed line in Fig. 3. The close-coupled values lie somewhat above those evaluated using Russek's model. However, this is expected since the crossing potentials are not linear in the region around R_x, as assumed in the parametrization of the model, but actually lie very close to one another, Fig. 1 and Table I. We therefore expect increased coupling and hence larger transition probabilities and inelastic total cross-sections for our case.

There also appears to be a hint of oscillatory structure on our cross sections, which correlates to the stationary phase region of the transition probabilities. The 8.65 and 10 eV cross sections lie somewhat farther above the dashed line than the 5 and 25 eV calculations indicating a possible maximum in the energy dependence of the cross sections. The 100 eV cross section deviates significantly above the estimates using Russek's method and this is due to added contribution to the transition probabilities from the inner crossing.

If we use Russek's method as a guide for extrapolating our inelastic total cross-sections to higher energies, we obtain a value of $Q \gtrsim 6 \times 10^{-16}$ cm^2 at 1000 eV. Comparing our results to the calculations of Ref. 3, where radial coupling was considered as inducing the

inelastic transitions, it is evident that rotational coupling will be the dominant inelastic process up to collision energies of at least 500 eV.

The inelastic direct excitation differential cross sections were evaluated from the real and imaginary parts of the S-matrix using the formulas

$$\sigma_{12}(\theta) = (A^2 + B^2)/(4k^2) \qquad (3)$$

where

$$A = \sum_{\text{even } \ell} (2\ell + 1)\ \mathrm{Re}(S_{12})\ P_\ell(\cos\theta) \qquad (4)$$

and

$$B = \sum_{\text{even } \ell} (2\ell + 1)\ \mathrm{Im}(S_{12})\ P_\ell(\cos\theta) \quad . \qquad (5)$$

The results of these calculations are shown in Fig. 4. The inelastic differential cross-sections are plotted to 90° and not to 180° since they are symmetric about 90°. The major characteristics of these cross-sections are a peak of large magnitude at small angles with superimposed rainbow structure and the prescence of nuclear symmetry oscillations at large angles.

A more convenient way to plot the inelastic differential cross-section is to use the reduced coordinates $\tau = E\theta$ and $\rho(\theta) = \theta \sin\theta\ \sigma(\theta)$. The rapid decrease in the cross-section is removed by using the reduced cross-section ρ. The reduced angle τ is convenient because it is inversely related to the impact parameter (large τ, low b; etc.). Utilizing this type of plot, there are two major peaks found in the forward scattering cross sections ($0^\circ < \theta < 90^\circ$). The largest peak is centered at about 100 eV-degrees, Fig. 5, and corresponds to the transition probabilities found for impact parameters in the range of about $b \approx 3.0\ a_0$, Fig. 2. The second peak (centered at τ = 175 eV-deg at 5 eV, 160 eV-deg at 8.65 eV, and 150 eV-deg at 10 eV) is a Stückelberg oscillation due to an interference caused by the two possible trajectories within R_x.

Superimposed on the cross sections displayed in Fig. 5 are fine structure oscillations due to inelastic rainbow scattering out of the deep $c^3\Pi_g$ potential well, $\epsilon \approx 2.2$ eV (Table I). This structure is prevalent only at small angles, $\tau \lesssim 300$ eV-deg, and at the larger angles nuclear symmetry oscillations are observed, Fig. 4. The nuclear symmetry oscillations are caused by the indistinguishability of the colliding particles and the fact that it is impossible to differentiate between direct excitation scattering at angle θ and excitation transfer from $\Pi-\theta$. The nuclear symmetry oscillations have their greatest magnitude at 90°. Similar sets of oscillations with the same interpretation also occur on low energy $He^+ + He(1^1S) \rightarrow He^+ + He(2^3S)$ inelastic differential cross sections.[11]

Another interesting phenomenon displayed on the cross sections of Fig. 5 is the energy dependence of the magnitude of the inelastic rainbow oscillations. The magnitude of the fine structure on the 5 eV and especially on the 25 eV cross sections is much less than that of the 8.65 and 10 eV cross sections. These magnitude fluctuations are caused by the region of stationary phase at $b \approx 1.5\ a_o$ in the transition probabilities, Fig. 2. The inelastic rainbow oscillations require inelastic scattering on the positive angle branch of the special deflection functions[12] for interference effects to occur between the trajectories scattering to a negative angle and a positive value of the same angle. For this system the positive angle scattering arises from impact parameters $b \approx 1.7\ a_o$. Therefore, the magnitude of the transition probabilities in the $b \approx 1.7\ a_o$ region, Fig. 2, can be directly correlated to the magnitude of the fine structure oscillations.

Elastic 2-state and 3-state differential cross section calculations were also performed to ascertain the effect of the inelastic channel on the elastic cross sections. In this calculation we employed an $a^3\Sigma_u^+$ potential that was compatible with rainbow scattering measurements[1], the latest spectroscopic analysis[13] on the $A^1\Sigma_u^+$ state, and the

calculations of Liu[14] on the well depth of He_2^+. The cross section formulas have been given previously.[11]

In Fig. 6 are shown the results of the elastic calculations with (3-state) and without (2-state) the inclusion of the $b^3\Pi_g$ inelastic channel. There is very little change in the position of the main rainbow from the $a^3\Sigma_u^+$ state at $\tau \approx 160$ eV-deg. At smaller angles, however, $25 \lesssim \tau \lesssim 125$ eV-deg, the inelastic channel considerably modifies the cross sections. This is due to the loss of elastic flux out of the $b^3\Sigma_g^+$ state and the "perturbation" structure caused by the inelastic transition.[12, 15, 16]

Conclusions

In conclusion, we have calculated the ab initio potential energy curves for the $c^3\Sigma_g$ state of $He(2^3S) + He(1^1S)$ and the $b^3\Pi_g$ state of $He(2^3P) + He(1^1S)$ along with the rotational coupling matrix element, L_y. It is found that the inelastic transition probabilities induced by rotational coupling between the $c^3\Sigma_g$ and $b^3\Pi_g$ molecular states are quite large even at low energies, 5 eV, and dominate the inelastic scattering up to at least 500 eV.

The inelastic total cross sections (the sum of both direct and exchange excitation) were calculated and found to range from 1.0×10^{-16} cm^2 at 5 eV to 4.0×10^{-16} cm^2 at 100 eV. The inelastic differential cross-sections were found to peak at a reduced angle τ of about 100 eV-deg. This has been confirmed by a recent experiment performed at 8.65 eV.[2] Nuclear symmetry oscillations were superimposed on the inelastic differential cross-sections at large angles. At small angles, $\tau \lesssim 300$ eV-deg, inelastic rainbow structure was observed. The elastic differential cross sections were also calculated and were found to be significantly altered by the inelastic channel in the angular region $25 \lesssim \tau \lesssim 125$ eV-deg.

REFERENCES

1. R. Morgenstern, D. C. Lorents, J. R. Peterson, and R. E. Olson, Bull. Am. Phys. Soc. 17, 1131 (1972); ibid, Phys. Rev. A (submitted).
2. R. E. Olson, R. Morgenstern, D. C. Lorents, J. C. Browne, and L. Lenamon, Phys. Rev. Letters (submitted).
3. S. A. Evans, J. S. Cohen, and N. F. Lane, Phys. Rev. A 4, 2235 (1971).
4. E. M. Greenawalt, Ph.D. Thesis (University of Texas, 1967) (unpublished).
5. D. J. Klein, E. M. Greenawalt, and F. A. Matsen, J. Chem. Phys. 47, 4820 (1967).
6. H. J. Kolker and H. H. Michels, J. Chem. Phys. 50, 1762 (1969).
7. M. J. Ginter and R. Battino, J. Chem. Phys. 52, 4469 (1970).
8. D. Secrest and B. R. Johnson, J. Chem. Phys. 45, 4556 (1966).
9. R. E. Olson, Phys. Rev. A 2, 121 (1970).
10. A. Russek, Phys. Rev. A 4, 1918 (1971).
11. R. E. Olson, Phys. Rev. A 5, 2094 (1972).
12. R. E. Olson and F. T. Smith, Phys. Rev. A 3, 1607 (1971); ibid, 6, 526 (1972).
13. K. M. Sando, Mol. Phys. 23, 413 (1972).
14. B. Liu, Phys. Rev. Letters 27, 1251 (1971).
15. F. T. Smith, D. C. Lorents, W. Aberth, and R. P. Marchi, Phys. Rev. Letters 15, 742 (1965).
16. R. P. Marchi, Phys. Rev. 183, 185 (1969).

Table I

Potential Energy Curves and Coupling Matrix Elements

R(ao) \ $E(a,u_g)$ ($^3\Sigma_g^a$)	$^3\Sigma_g^b$	$^3\pi_g^a$	$\langle {}^3\Sigma_g \mid L_y \mid {}^3\pi_g \rangle$
1.0	-4.40σσ43	-4.408026	0.937885
1.5	-4.989949	-5.027520	0.898538
1.75	-5.063993	-5.090993	0.893320
2.0	-5.089264	-5.115047	0.890965
2.5	-5.085316	-5.103260	0.879553
3.0	-5.070398	-5.05483	-5.078246	0.839906
3.25	-5.067055	-	-5.067487	0.799513
3.5	-5.065814	-5.05483	-5.058907	0.750614
3.75	-5.066228	-5.052358	0.706118
4.0	-5.067162	-5.05943	-5.047515	0.664079
5.0	-5.072013	-5.06553	-5.038799	0.549118
6.0	-5.075204	-5.06913	-5.036836
8.0		-5.036368
10.0	-5.078784	-5.07223	-5.036411
15.0	-5.078949	-5.035280

a) This calculation adjusted by the procedure of ref. 5

b) text ref. 6.

Table II

INELASTIC TOTAL CROSS SECTIONS

Energy-eV	$Q - 10^{-16}$ cm^2
5	1.04
8.65	1.42
10	1.45
25	2.05
100	4.0

FIGURE CAPTIONS

1. Potential curves from Ginter and Battino (Ref. 7) leading to the separated atom limits of $He(2^3S) + He(1^1S)$ and $He(2^3P) + He(1^1S)$.

2. Transition probabilities vs. impact parameter for the collision energies of 5, 8.65, 10, 25, and 100 eV. At 100 eV the calculations were performed at a wide grid of impact parameters, these points are depicted by the solid circles. To calculate the total inelastic cross section, the 100 eV transition probabilities were crudely interpolated. This uncertainty is illustrated by the dashed line.

3. Calculated rotational inelastic total cross sections; solid circles. The calculations of Evans, Cohen, and Lane (Ref. 3) for radial coupling are shown by the solid squares. An estimate of the rotational inelastic total cross sections using the method of Russek (Ref. 10) and our potential parameters (Table I) is given by the dashed line.

4. Inelastic differential cross sections as a function of angle for the collision energies of 5, 8.65, 10, and 25 eV.

5. Reduced inelastic differential cross sections $\rho = \theta \sin\theta\sigma\theta$ as a function of reduced angle $\tau = E\theta$ for the collision energies of 5, 8.65, 10, and 25 eV.

6. Reduced elastic differential cross sections ρ as a function of reduced angle τ. The dashed line is a 2-state calculation using the adiabatic potentials $a^3\Sigma_u^+$ and $c^3\Sigma_g^+$ that lead to $He(2^3S) + He(1^1S)$. The solid line is a 3-state calculation that includes the $b^3\Pi_g$ inelastic channel.

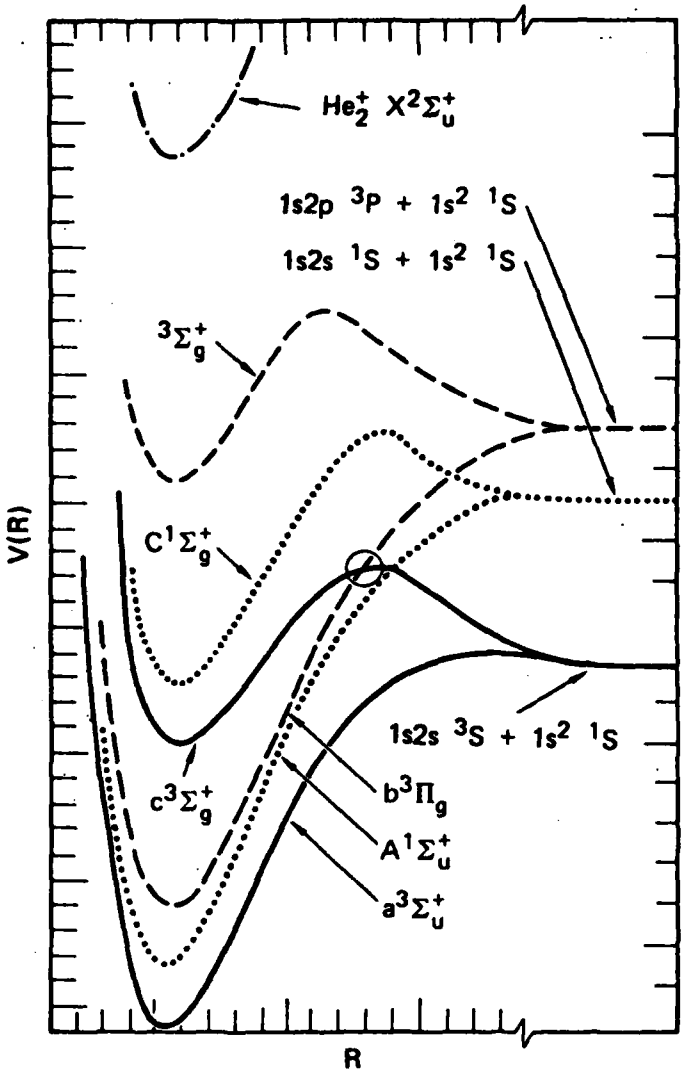
$He_2^+ X^2\Sigma_u^+$
1s2p ^3P + 1s^2 ^1S
1s2s ^1S + 1s^2 ^1S
$^3\Sigma_g^+$
$C^1\Sigma_g^+$
$c^3\Sigma_g^+$
1s2s ^3S + 1s^2 ^1S
$b^3\Pi_g$
$A^1\Sigma_u^+$
$a^3\Sigma_u^+$
V(R)
R

Figure 1

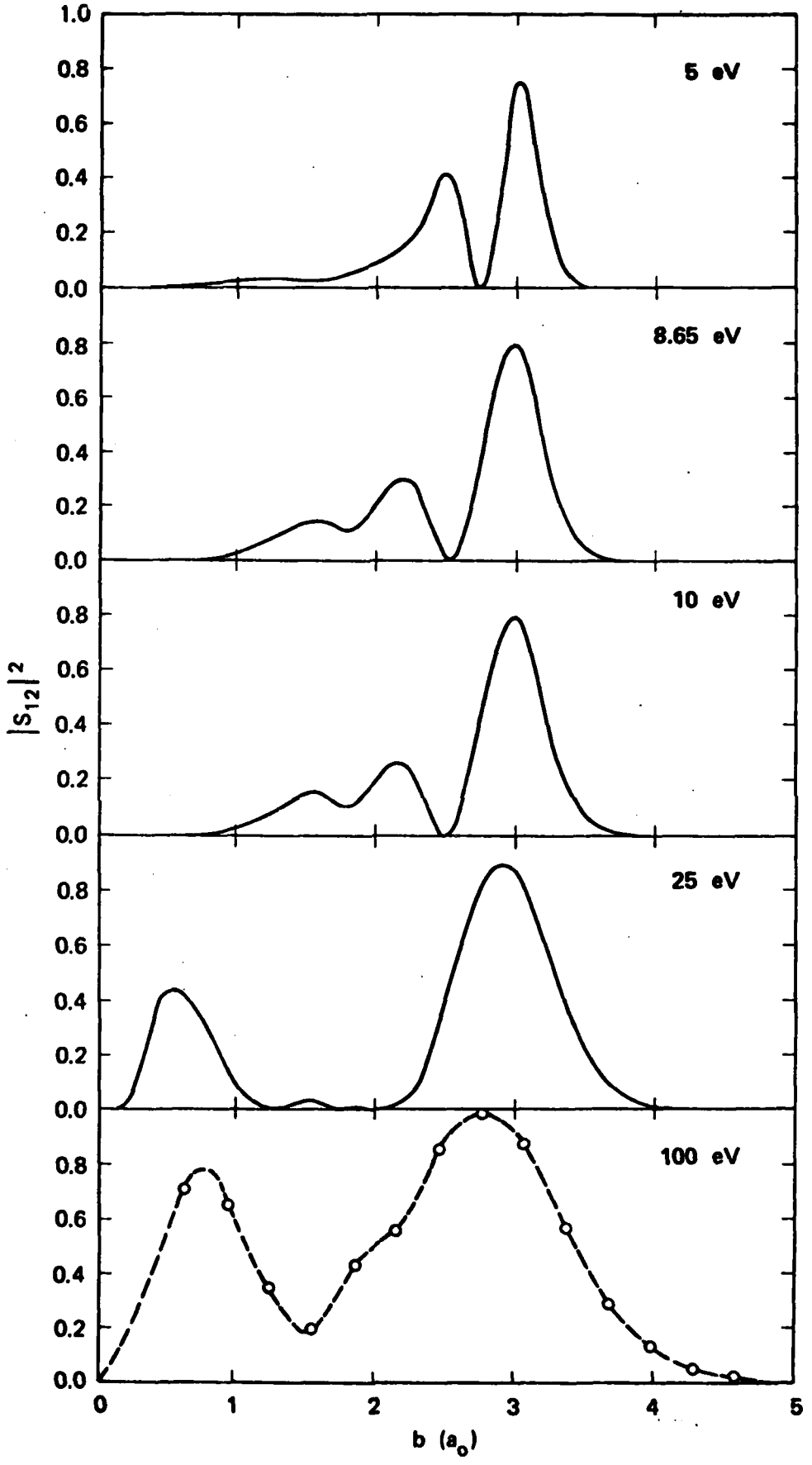

Figure 2.

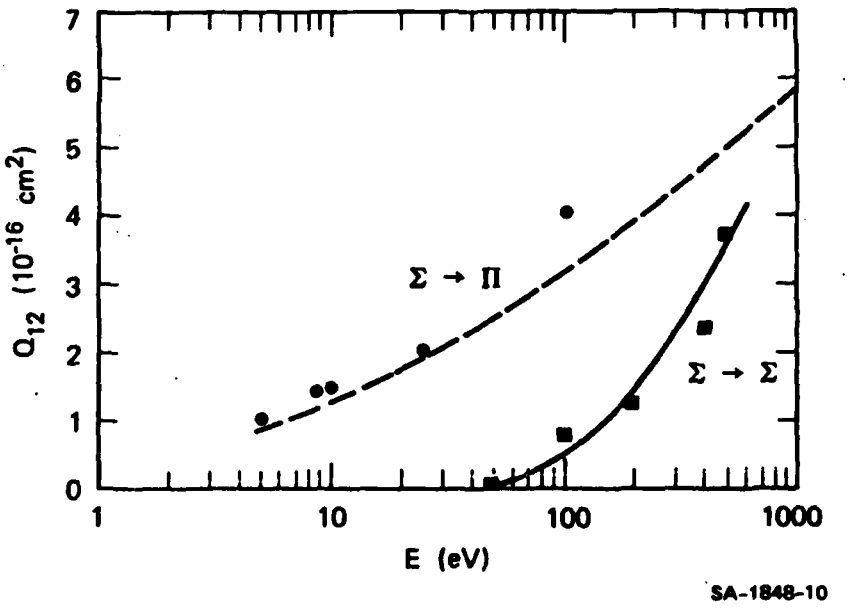
7
6
5
4
3
2
1
0
Q_{12} (10^{-16} cm^2)
$\Sigma \rightarrow \Pi$
$\Sigma \rightarrow \Sigma$
1
10
100
1000
E (eV)
SA-1848-10

Figure 3.

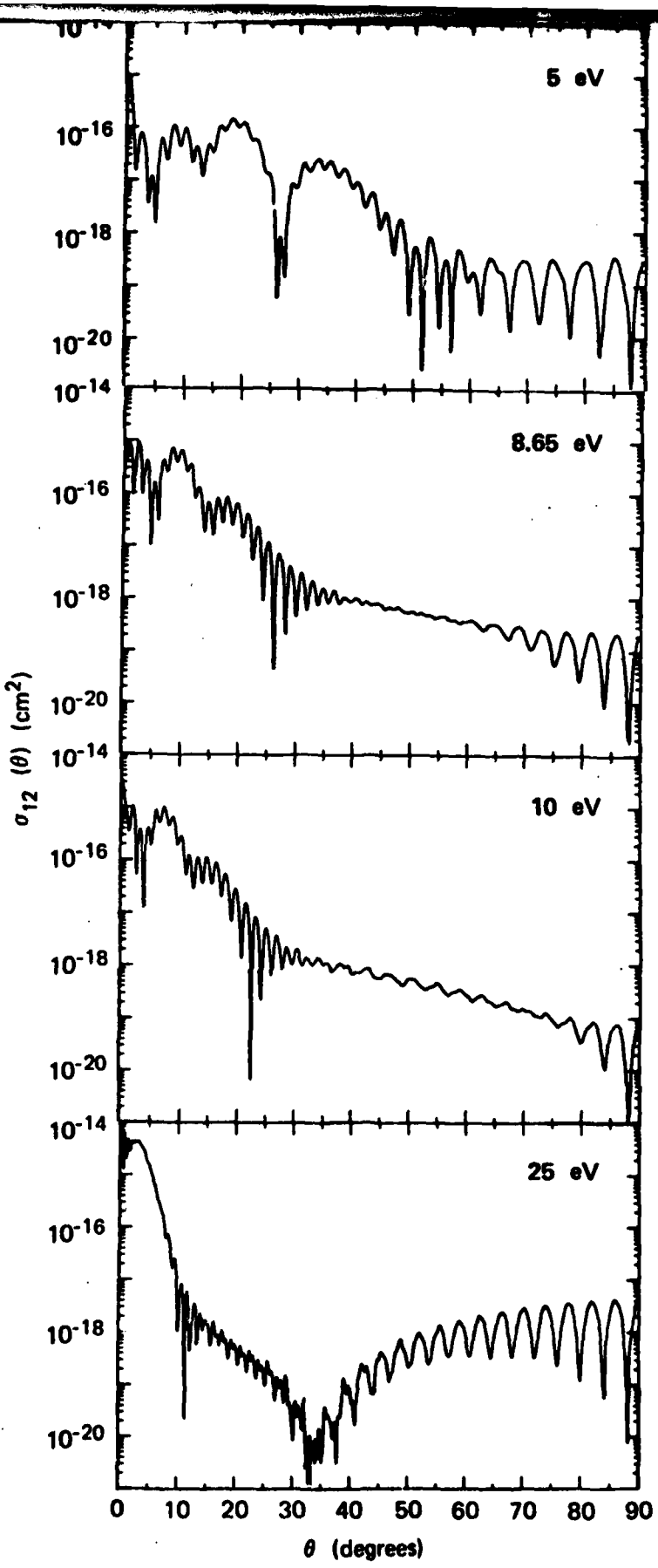
5 eV
8.65 eV
10 eV
25 eV
10^{-16}
10^{-18}
10^{-20}
10^{-14}
σ_{12} (θ) (cm^2)
0 10 20 30 40 50 60 70 80 90
θ (degrees)

Figure 4.

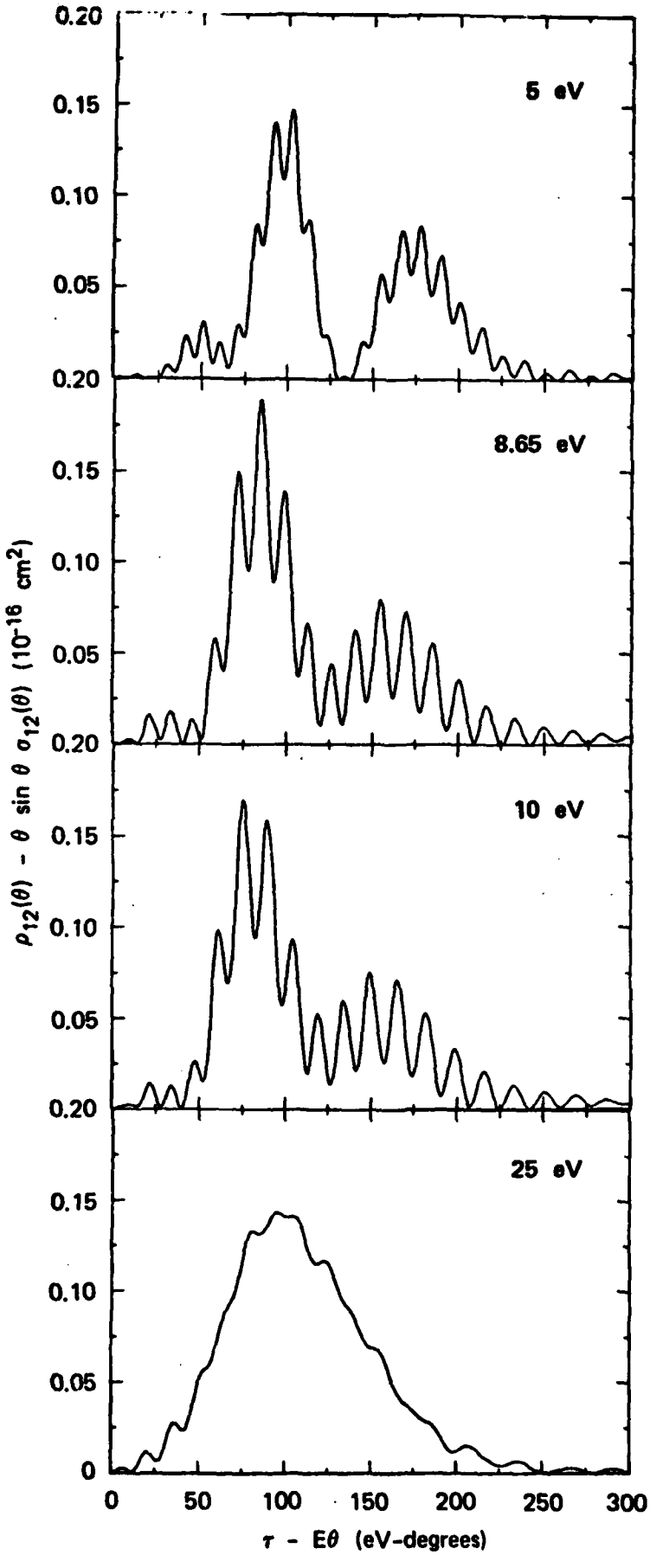
5 eV
8.65 eV
10 eV
25 eV
0.20
0.15
0.10
0.05
0
0 50 100 150 200 250 300
τ - Eθ (eV-degrees)
ρ12(θ) - θ sin θ σ12(θ) (10-16 cm2)

Figure 5.

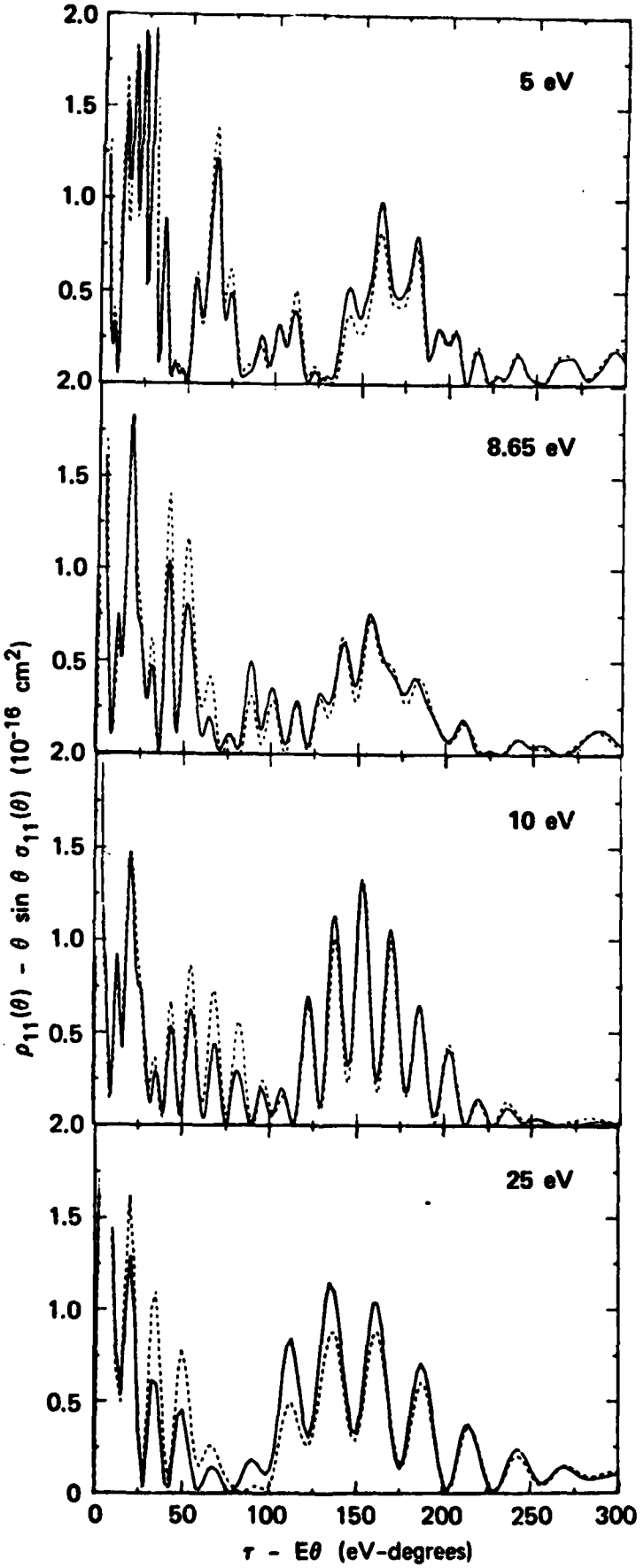
5 eV
8.65 eV
10 eV
25 eV
2.0
1.5
1.0
0.5
0
0
50
100
150
200
250
300
$\rho_{11}(\theta) - \theta \sin\theta\, \sigma_{11}(\theta)$ $(10^{-16}$ cm$^2)$
$\tau - E\theta$ (eV-degrees)

Figure 6.

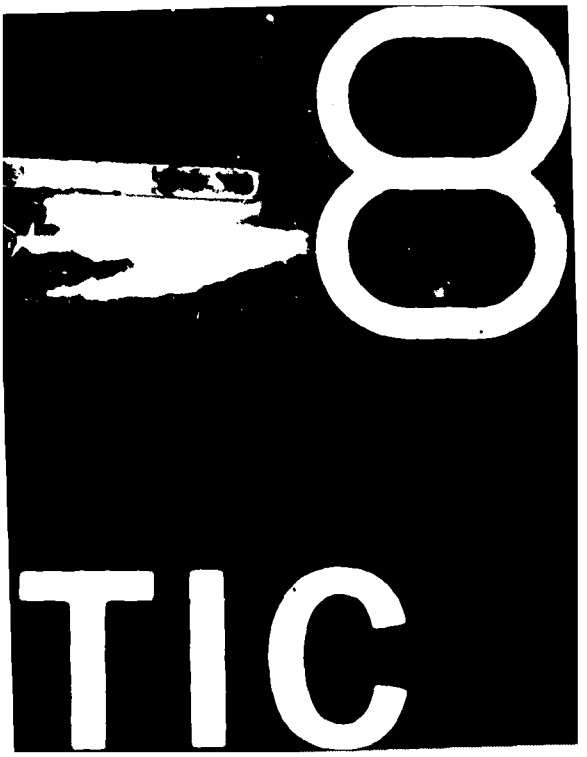
8
TIC